JOURNAL OF GEOPHYSICAL RESEARCH, VOL. 96, NO. D5, PAGES 9159-9168, MAY 20, 1991

Effects of Surface Temperature and Clouds on the CO_2 Forcing

CHRISTINA SCHMITT AND DAVID A. RANDALL

Department of Atmospheric Science, Colorado State University, Fort Collins

CO_2 forcing is defined as the initial change in heating rate, with no feedbacks included, that is the direct response to an increase in the CO_2 concentration in the atmosphere. We have conducted a study of the effects of surface temperature and clouds on the CO_2 forcing, based on use of the Colorado State University general circulation model. We report results from a pair of perpetual July simulations in which the sea surface temperatures differ by 4 K. The precipitable water is about 1.5 times larger in the warm run. The increased water vapor concentration amplifies the radiative effects of CO_2, leading to greater CO_2 forcing in the warm run. In the colder run the globally averaged reduction in upward longwave radiation due to a doubling of CO_2 is 4.3 W m^{-2} at the level of maximum forcing, or the "CO_2 tropopause." Above and below this level the CO_2 forcing decreases, resulting in a net tropospheric warming of 3.3×10^{-2} K day^{-1}, and a net stratospheric cooling. In the warm run the CO_2 forcing at the CO_2 tropopause is 4.6 W m^{-2}, and is associated with a tropospheric warming of $4. \times 10^{-2}$ K day^{-1}. The clear-sky CO_2 forcing at the CO_2 tropopause is 5.0 W m^{-2} in the cold run, and 5.2 W m^{-2} in the warm run. By blocking infrared radiation that would otherwise be blocked by CO_2, the clouds reduce the CO_2 forcing of the surface-troposphere system by 0.66 W m^{-2} in the cold run, and by 0.59 W m^{-2} in the warm run. Our results for the CO_2 forcing are model-dependent, of course. Every GCM-based study of CO_2-induced climate change produces a CO_2 forcing, however, and the warming scenarios generated depend very directly on this forcing. A thorough investigation of the CO_2 forcings produced by GCMs is thus a rather basic prerequisite for understanding the climate change predictions produced by the models.

INTRODUCTION

Global warming is a predicted consequence of increasing greenhouse gas concentrations [*Intergovernmental Panel on Climate Change* (IPCC), 1990]. These predictions are based primarily on general circulation model (GCM) simulations, which entail many uncertainties. We have investigated a particular and rather basic element of the greenhouse warming theory: the CO_2 forcing. This is defined as the initial change in heating rate (with no feedback effects included) that is the direct response to an increase in the CO_2 content of the atmosphere. The CO_2 forcing is a logical starting point for understanding the greenhouse effect on the Earth's atmosphere.

Ramanathan et al. [1979] investigated the zonal and seasonal variations in radiative fluxes and surface temperature due to increased CO_2. Their study made use of both a radiative convective model and an energy balance model, in a three-step procedure. First, the tropospheric temperatures were held fixed (at the observed values), and the response of the stratosphere to CO_2 forcing was determined. Next, the radiative heating of the surface-troposphere system due to increased CO_2 was obtained. Finally, the computed radiative heating was used in an energy balance model to estimate the changes in surface temperature due to the increased CO_2.

Their results showed that the tropospheric CO_2 forcing is greatest at the equator, and decreases poleward, and that it is strongest in the summer and weakest in the winter. They concluded that the differences in CO_2 heating rates were caused by the exponential decrease of the CO_2 absorption as the temperature increases. They also showed that the stratospheric contribution to the CO_2 forcing increases toward the poles (because the tropopause is relatively low near the poles), and that the surface heating due to the CO_2 forcing also increases poleward.

They also presented overcast and clear-sky values for the tropospheric and surface heating, based on the early cloud data set compiled by London. They found that the clouds reduce the CO_2 forcing at the Earth's surface but increase the CO_2 forcing of the troposphere.

Although *Ramanathan et al.* [1979] provided useful insights into the nature of the CO_2 forcing, the problem deserves further attention for a number of reasons. Their representation of the atmosphere was highly simplified, and the cloud data set that they used was rather crude by modern standards. A GCM-based study of the CO_2 forcing is particularly appropriate, since GCMs are the tools used to predict the climatic consequences of CO_2 forcing. A GCM study can provide a comprehensive view of the CO_2 forcing, including, for example, the complicated effects of the land-sea distribution, the diurnal cycle, and model-generated clouds. In addition, a GCM-based CO_2 forcing study can serve as the foundation for a climate change simulation using the same model.

We decided to investigate the effects of surface temperature and cloudiness on the CO_2 forcing. The temperature-dependence of the CO_2 forcing can provide clues to the feedback that a warming exerts on the forcing that produces it. As discussed below, this feedback occurs largely through the increase in atmospheric water vapor concentrations at higher temperatures [*Ramanathan*, 1981].

The role of clouds is probably the least understood aspect of the greenhouse warming theory. As is well known, clouds produce two opposing effects on the Earth's radiation budget: the absorbed solar radiation decreases with increased cloud amount, while the outgoing terrestrial radiation decreases. Clouds also influence the surface energy budget, through cloud shadows, by downward emission of infrared radiation from cloud base and by blocking downward infrared radiation emitted above the level of the cloud. Through

Paper number 91JD00685.
0148-0227/91/91JD-00685$05.00

TABLE 1*a*. Results of a Test Calculation in Which the Temperature of the "Stratosphere" Above 50 mbar is Assumed to be the Same as the Temperature of the Top Layer of the Model, in this Case 179 K

	$1 \times CO_2$			$2 \times CO_2$			CO_2 Forcing		
L	$F\uparrow$	$F\downarrow$	F	$F\uparrow$	$F\downarrow$	F	$F\uparrow$	$F\downarrow$	F
1	288.90	0.00	−288.90	284.66	0.00	−284.66	−4.24	0.00	4.24
2	290.25	3.02	−287.23	286.05	3.64	−282.41	−4.20	0.63	4.82
3	291.85	4.90	−286.95	287.89	5.90	−281.99	−3.96	0.99	4.95
4	294.69	8.29	−286.39	291.16	9.85	−281.31	−3.52	1.56	5.08
5	299.28	14.32	−284.96	296.43	16.65	−279.78	−2.85	2.33	5.18
6	305.76	23.77	−281.98	303.85	27.02	−276.83	−1.91	3.25	5.16
7	329.28	124.69	−204.59	328.16	128.23	−199.93	−1.12	3.54	4.66
8	355.01	179.86	−175.15	354.52	183.46	−171.07	−0.48	3.60	4.08
9	390.59	261.72	−128.87	390.48	263.77	−126.71	−0.11	2.05	2.16
10	441.65	373.40	−68.25	441.54	373.64	−67.90	−0.11	0.24	0.35
11	453.01	399.65	−53.36	453.01	399.87	−53.14	0.00	0.22	0.22

A GATE sounding was used to specify the temperature and moisture profiles from the surface up to 50 mbar. Clear skies were assumed. Upward, downward, and net upward infrared fluxes are denoted by $F\uparrow$, $F\downarrow$, and F, respectively. All units are W m^{-2}. All fluxes are defined at the "edges" of model layers. Nine model layers are used, together with the prescribed "stratosphere" layer, giving a total of 10 layers. These 10 layers have 11 edges. The index L, given in the first column of the table, counts from the "top of the atmosphere" (L = 1), to the Earth's surface (L = 11). The pressure at L = 3 is 100 mbar, which is near the CO_2 tropopause.

these various effects, the clouds can modulate the CO_2 forcing.

EXPERIMENT DESIGN

We have used the Colorado State University (CSU) general circulation model, which is a modified version of the University of California, Los Angeles (UCLA) GCM developed by Arakawa and colleagues. An up-to-date description of the CSU model has recently been published by *Randall et al.* [1989]; only a brief summary is given here.

The equations are horizontally finite-differenced on a staggered latitude-longitude grid, with a grid spacing of 4° latitude by 5° longitude. The version of the model used here has nine layers, with its top at the 50-mbar level. The lowest layer is identified as the planetary boundary level (PBL), through the use of a modified sigma coordinate system. The diurnal cycle is included. Terrestrial radiation is parameterized as described by *Harshvardhan et al.* [1987]. This scheme is a combination of several broadband schemes, producing a balance of accuracy and computationally fast parameterization suited for GCMs. The effects of H_2O, CO_2, and O_3 are included. The CO_2 bands included are in the spectral range of 13.9–16.1 μm, with wings out to 12.5 and 18.5 μm. The spectral integration is approximated by the methods of *Chou and Peng* [1983] for the CO_2 bands, and *Chou* [1984] for the H_2O band. The overlap region of the water vapor continuum and the line absorption due to H_2O, CO_2, and O_3, using the method of *Roberts et al.* [1976], is also included.

Clouds can form in any layer of the GCM. They are associated with PBL stratocumulus clouds, large-scale saturation, or the anvils of deep cumulus clouds. Convective "anvil" clouds are assumed to occur when convection, parameterized following *Arakawa and Schubert* [1974], penetrates above 400 mbar. These anvil clouds are representative of optically and geometrically thick upper level cloud masses. The cloud fills the grid column horizontally, from 400 mbar up to the level reached by the convection. The convective cloudiness is assumed to be negligible below 400 mbar. Supersaturation clouds form when the relative humidity reaches 100%, and are assumed to fill the grid cells both horizontally and vertically. Upper level supersaturation clouds represent cirrus clouds. Boundary layer clouds are detected when the relative humidity at the PBL top exceeds 100%. Their cloud base occurs where the relative humidity is exactly 100%. Their cloud fraction is assumed to be 1 when they are more than 12.5 mbar deep, and to decrease linearly to zero as their pressure thickness decreases from 12.5 mbar to zero. The radiative effects of the clouds are incorporated through prescribed, temperature-dependent cloud optical properties [*Harshvardhan et al.*, 1989].

To evaluate the CO_2 forcing, the radiation code is run twice; once with a CO_2 mixing ratio of 330 ppm, and a second time with 660 ppm. The CO_2 forcing is then obtained as the difference in the longwave radiation fields between these two cases. It is important to note that only the longwave heating rates obtained for 330 ppm are actually used in the model; the results obtained for 660 ppm are purely diagnostic.

Many diagnostics have been saved for both $1 \times CO_2$ and $2 \times CO_2$. These include the all-sky and clear-sky longwave radiation at both the Earth's surface and the CO_2 tropopause. We define the CO_2 tropopause as the level for which the difference in the upward infrared flux between $1 \times CO_2$ and $2 \times CO_2$ is maximized, that is, the level where the CO_2-induced reduction of the net upward longwave radiation is greatest. The all-sky and clear-sky pressures of the CO_2 tropopause are saved as diagnostics. Clear-sky fluxes are determined using method 2 of *Cess and Potter* [1987]; see also *Harshvardhan et al.* [1989].

The model is incapable of simulating the CO_2 forcing of the stratosphere (or, for that matter, any other property of the stratosphere), because its top is at 50 mbar and there is only one layer between 100 and 50 mbar. As an upper boundary condition for the longwave radiation parameterization, the downward longwave radiation at 50 mbar is determined using the assumption that the atmosphere above that level is isothermal with the same temperature as the top layer of the model [*Harshvardhan et al.*, 1987]; this leads to a severe underestimation of the effective radiative temperature of the stratosphere. Table 1 illustrates the consequences of this assumption, for a test case based on GATE data with

TABLE 1*b*. Same as Table 1*a*, Except That the Temperature of the "Stratosphere" Above 50 mbar is Assumed to be 225 K

	1 × CO_2			2 × CO_2			CO_2 Forcing		
L	$F\uparrow$	$F\downarrow$	F	$F\uparrow$	$F\downarrow$	F	$F\uparrow$	$F\downarrow$	F
1	294.99	0.00	−294.99	292.21	0.00	−292.21	−2.77	0.00	2.77
2	294.50	9.31	−285.19	291.51	11.49	−280.02	−2.99	2.18	5.17
3	291.85	8.38	−283.47	287.89	9.81	−278.08	−3.96	1.43	5.39
4	294.69	10.17	−284.51	291.16	11.83	−279.33	−3.52	1.65	5.18
5	299.28	15.57	−283.70	296.43	17.93	−278.50	−2.85	2.36	5.21
6	305.76	24.74	−281.02	303.85	28.00	−275.85	−1.91	3.26	5.17
7	329.28	124.78	−204.50	328.16	128.33	−199.84	−1.12	3.55	4.67
8	355.01	179.89	−175.11	354.52	183.49	−171.03	−0.48	3.60	4.08
9	390.59	261.73	−128.86	390.48	263.78	−126.70	−0.11	2.05	2.16
10	441.65	373.40	−68.25	441.54	373.64	−67.90	−0.11	0.24	0.35
11	453.01	399.65	−53.36	453.01	399.87	−53.14	0.00	0.22	0.22

the assumption of clear skies. To generate the results shown in Table 1*a*, the temperature of the air above 50 mbar is assumed, as in the GCM, to be equal to the temperature of the layer between 100 and 50 mbar, which in this case is a very cold 179 K. Similarly cold temperatures are typically produced in GCM runs with nine levels and the top at 50 mbar; this simply illustrates that such a model is (not surprisingly) incapable of simulating the observed thermal structure of the stratosphere. Table 1*a* gives the upward, downward, and net upward infrared radiation for 1 × CO_2, 2 × CO_2, and the CO_2 forcing. Table 1*b* gives the corresponding results for the case in which the air above 50 mbar is assumed to have a temperature of 225 K, close to the effective radiative temperature of the real stratosphere. In Table 1*a*, the CO_2 forcing of the stratosphere is a cooling of $4.24 - 4.95 = -0.71$ W m^{-2}, while in Table 1*b* it is $2.77 - 5.39 = -2.62$ W m^{-2}. The latter cooling rate is close to that expected based on more realistic troposphere-stratosphere radiative transfer models [e.g., *Ramanathan et al.*, 1979], while the former cooling rate is much too small. Note, however, that the CO_2 forcing of the troposphere is practically the same in both cases. This example illustrates that the assumed radiative upper boundary condition used in the GCM is of little or no practical consequence for tropospheric simulations, but completely precludes any quantitative discussion of the stratospheric CO_2 forcing. For this reason, we do not (cannot) use our model results to draw inferences about the effects of the CO_2 forcing on the stratosphere or the outgoing longwave radiation at the "top of the atmosphere." We confine ourselves to a discussion of the CO_2 forcing of the surface-troposphere system.

The GCM results presented here are taken from the same "perpetual July" runs used in the GCM intercomparison study discussed by *Cess et al.* [1989, 1990]. Cess et al. reported on two model runs. In the first, the sea surface temperatures (SSTs) were set to 2 K below the normal July 15 values, and in the second run they were set to 2 K above the normal July 15 values. We refer to these as the cold run and the warm run, respectively.

For each run, the results presented in this paper are averaged over 60 days following a 30-day spin-up, starting from July 15 conditions taken from the middle an earlier, multiyear, seasonal simulation with the same version of the model. We have found that the CO_2 forcing results are very insensitive to the averaging interval.

RESULTS

General Response to Surface Warming

Before turning to the CO_2 forcing results, we first briefly discuss the differences between the two model runs.

In the cold run, the atmospheric temperature varies from 294 K at the surface near the equator, to 186 K above 14-km altitude in the winter hemisphere. Figure 1 shows the latitude-height distribution of the differences in temperature between the warm run and the cold run. For obvious reasons, the warm run has near-surface temperatures about 4 K warmer than those of the cold run. The temperature difference increases with altitude up to about 6 or 7 km near the poles, and up to about 13 km in the tropics. The largest temperature difference is about 10.8 K near the 13-km (200 mbar) level in the tropics.

This strong warming of the tropical upper troposphere is characteristic of the model's penetrative convection scheme, and it is qualitatively similar to the temperature changes seen in greenhouse warming simulations based on other models

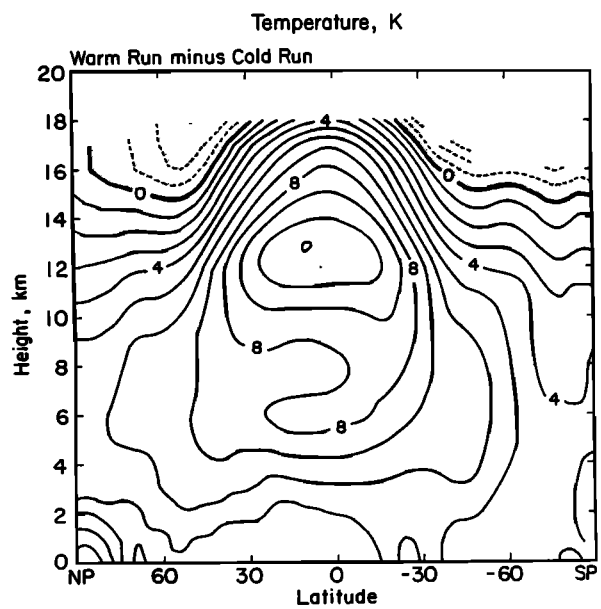

Fig. 1. Latitude-height plot of the zonally averaged temperature difference between the warm run and the cold run.

that use penetrative convection schemes [*Schlesinger and Mitchell*, 1987]. An explanation is as follows. Moist convection tends to limit the degree of conditional instability in an atmospheric column, by consuming the moist available energy (MAE) that is generated by such nonconvective processes as radiative cooling and moisture convergence. When we increase the SST in the warm run, this tends to change the MAE. As discussed by *Arakawa and Chen* [1987], increased MAE is favored by greater low-level humidity and a steeper lapse rate of temperature. Deep, penetrative convection "feels" the lapse rate through the entire depth of the troposphere. In order to prevent the increased water vapor of the warm run from producing a huge increase in the MAE, convective heating must cause the lapse rate to decrease, that is, it must warm the upper troposphere more than the lower troposphere. This accounts for the pattern seen in Figure 1.

Figure 2 shows the zonally averaged precipitable water (vertically integrated water vapor amount) for the cold run, and the difference in the precipitable water between the warm and cold runs. The global mean is about 21 mm in the cold run, and about 30 mm in the warm run (about a 50% increase). The maximum near the equator is about 30 mm in the cold run and about 45 mm in the warm run.

In the cold run the zonally averaged specific humidity (not shown) has a maximum of 9.6 g kg^{-1} at the surface at about 5°S, and decreases poleward and upward. The zonally averaged specific humidity is greater in the warm run, at every level and every latitude; the maximum in the warm run is about 14 g kg^{-1}. The enhanced convection of the warmer run (discussed below) transports water vapor into the middle and upper troposphere, thus moistening those regions. The relative humidity is also greater in the warm run, except in the tropics from about 4–10 km, where the strong convective warming dominates the increased specific humidity.

The evaporation rate reaches a maximum of 5.2 mm d^{-1} at the equator in the cold run. The global means of the evaporation and precipitation rates are 3.54 mm d^{-1} in the cold run and 4.29 mm d^{-1} in the warm run. The "speed" of the hydrologic cycle thus increases by about 25%, in response to the 4 K SST warming. The precipitation differences between the warm and cold runs generally increase from the poles toward the equator, except for minima in the subtropics. The hydrologic cycle simulated by the CSU GCM has been discussed in much more detail in recent papers by *Randall et al.* [1989, 1991].

The zonally averaged high (above 400 mbar) cloud amount is shown in Figure 3. The global mean of the high cloud amount is 0.53 in the cold run, and 0.51 in the warm run. A strong peak in the zonally averaged high cloudiness occurs near the equator, reaching ~0.75 in the cold run and ~0.68 in the warm run. Weaker maxima occur in mid-latitudes.

The boundary layer stratus (Figure 4) make up the majority of low clouds (below 700 mbar). The simulated stratus incidence is greatest at about 60°N and 60°S, and has a minimum in the tropics. The globally averaged low cloud amount decreases from 0.24 in the cold run to 0.22 in the warm run.

The simulated middle cloud amount (between 700 and 400 mbar) has global means of 0.21 in the cold run, and 0.17 in the warm run. Its distribution resembles that of low clouds, with maxima at higher latitudes (~0.50), and a minimum near the equator (~0.05).

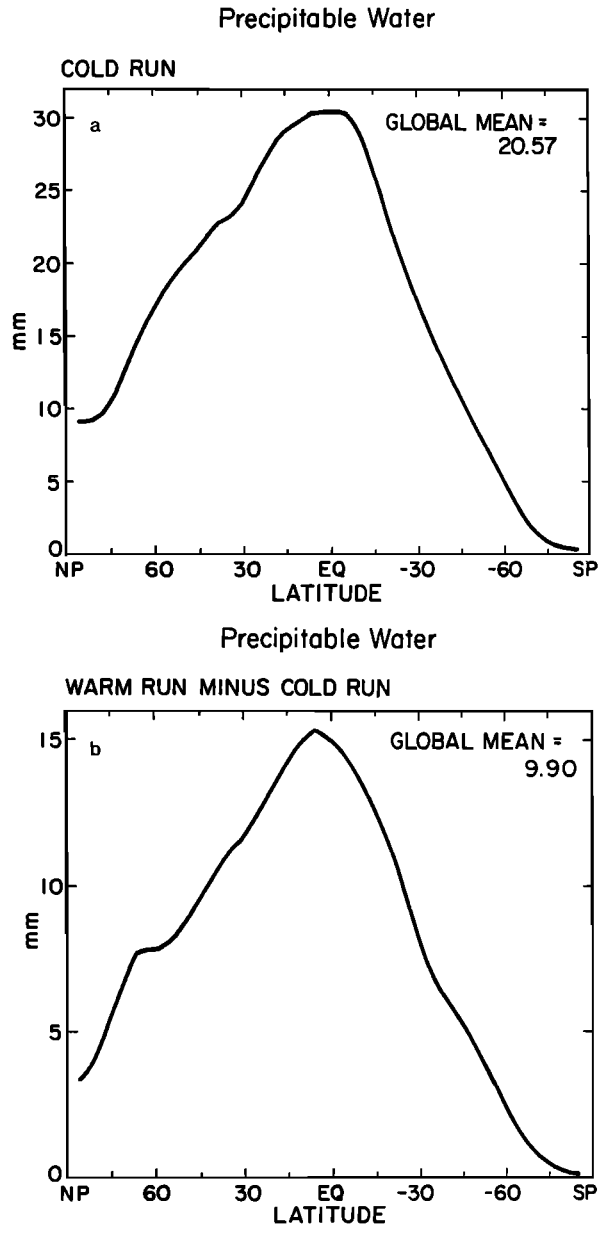

Fig. 2. Zonally averaged precipitable water for (*a*) the cold run, and (*b*) the warm run minus the cold run.

In summary, the warm run produces less cloudiness at all levels. Many 2 × CO_2 simulations also show less cloud than their 1 × CO_2 controls [*Schlesinger and Mitchell*, 1987; IPCC, 1990]. A much more detailed analysis of the cloudiness simulated by the CSU GCM is given by *Harshvardhan et al.* [1989].

Figures 5 and 6 show the latitude-height distribution of the infrared radiative heating rate for the cold run, and the differences between the warm cold runs, respectively. The longwave cooling of the atmosphere is generally stronger in the warm run, because the emitted infrared radiation increases with temperature, because the increased water vapor in the warm run emits more radiation, and also because, as discussed later, there are fewer clouds in the warm run. The cooling is most intense near the surface in the tropics, where the water vapor continuum dominates, and in the middle latitudes of the summer hemisphere. The clear-sky

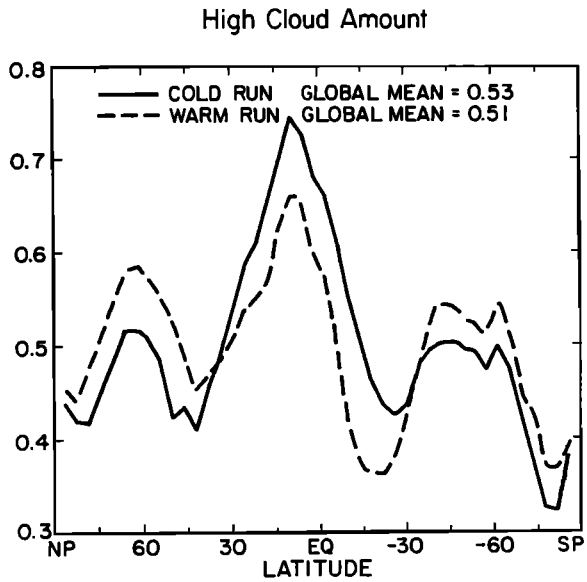

Fig. 3. Zonally averaged high cloudiness for the cold run and the warm run.

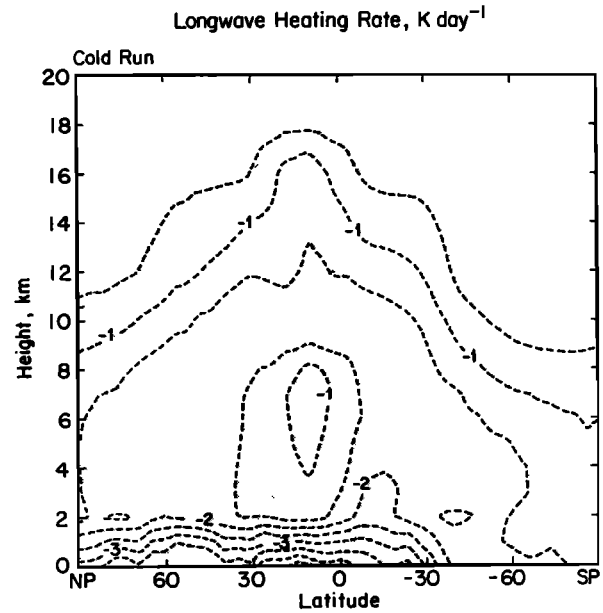

Fig. 5. Latitude-height distribution of longwave heating rate for the cold run.

atmospheric infrared cooling rate (not shown) is also generally stronger in the warm run, and the difference in clear-sky cooling between warm and cold runs is greatest in the tropics at high levels.

The global means for net longwave flux at the surface for the cold run and the warm run are 68 and 60 W m^{-2}, respectively; the corresponding clear-sky values are 95 W m^{-2} in the cold run and 83 W m^{-2} in the warm run. Note that the warm run actually experiences less surface infrared cooling; this is due to the water vapor feedback, as explained by *Ramanathan* [1981]. The zonally averaged surface IR cooling peaks in the summer hemisphere subtropics: 90 W m^{-2} in the cold run and 77 W m^{-2} in the warm run. The clear-sky IR surface cooling strongly peaks in the winter hemisphere mid-latitudes. The lack of this peak in the all-sky case can be attributed to middle and low level clouds.

The global mean of the outgoing longwave radiation at the top of the atmosphere is 220 W m^{-2} in the cold run and 234 W m^{-2} in the warm run. The corresponding clear-sky values are 254 and 265 W m^{-2} for the cold run and the warm run, respectively. The planetary radiation budget simulated by the CSU GCM is discussed in detail by *Harshvardhan et al.* [1989].

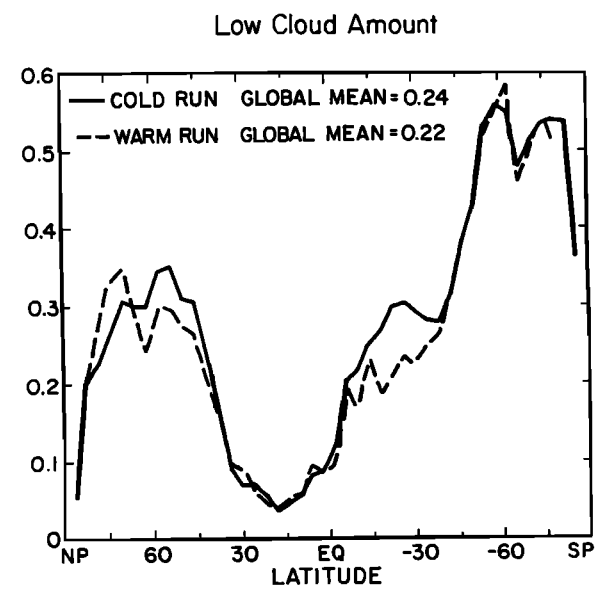

Fig. 4. Zonally averaged stratus incidence for the cold run and the warm run.

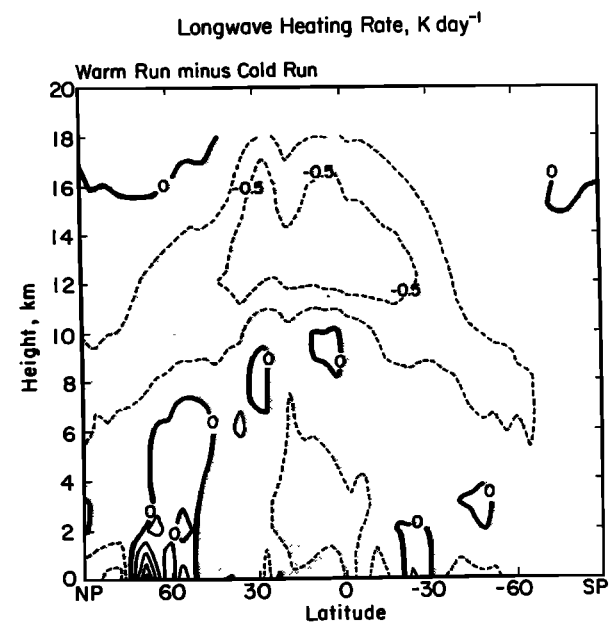

Fig. 6. Latitude-height differences (warm run minus cold run) in the longwave heating rate.

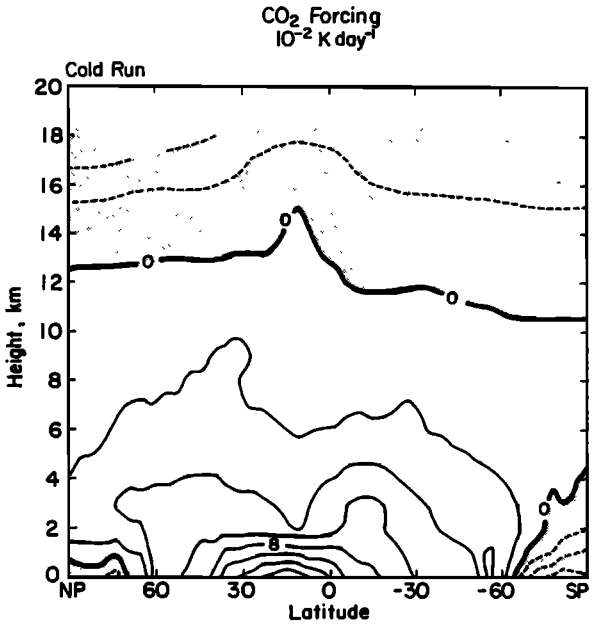

Fig. 7. Latitude-height distribution of the CO_2 forcing for the cold run.

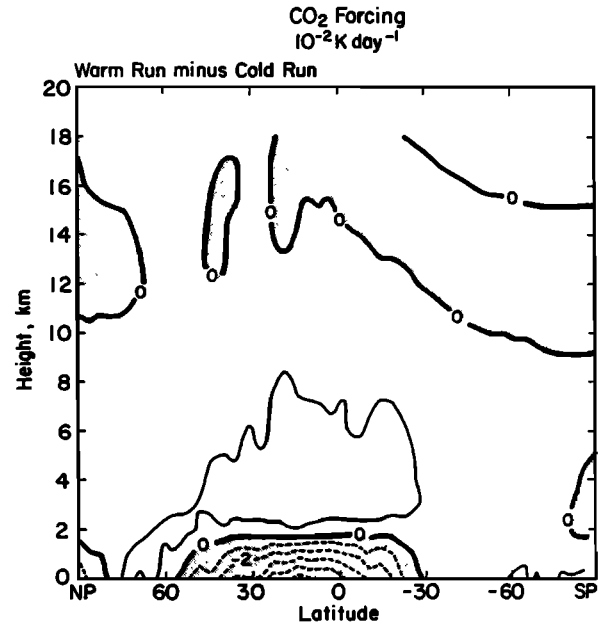

Fig. 8. Latitude-height differences (warm run minus cold run) in the CO_2 forcing.

CO_2 Forcing

Figure 7 shows the latitude-height distributions of infrared cooling due to CO_2 forcing ($2 \times CO_2 - 1 \times CO_2$) for the cold run. The CO_2 forcing tends to warm the troposphere, and it is most intense at lower levels in the tropics. In the cold run, the CO_2 forcing reaches 0.16 K d^{-1} near the surface at 15°N, while in the warm run, it reaches only 0.10 K d^{-1}. The CO_2-induced warming extends to particularly high levels in the tropics, owing to the effects of deep penetrative clouds. The CO_2 tropopause can be clearly seen in Figure 7 as the level (near 12 km) at which tropospheric warming gives way to stratospheric cooling. There is a peak in the height of the CO_2 tropopause in the tropics. As discussed below, this is due to the effects of high clouds. The CO_2 forcing actually tends to cool near the surface at high latitudes because of temperature inversions. Cooling reaches about 0.07 K d^{-1} near the surface at the winter pole, in both runs.

Figure 8 shows that the tropospheric CO_2 forcing is stronger in the warm run, except near the surface in the tropics, where it is stronger in the cold run. The increased water vapor content of the warm run leads to absorption of the down-welling radiation emitted by upper tropospheric CO_2 at a higher level; less of this radiation penetrates to the lower troposphere. For this reason, the warming tendency due to CO_2 forcing shifts upward in the warm run, relative to the cold run.

The tropospheric and surface CO_2 forcing and their temperature dependence are strongly influenced by the effects of water vapor. As discussed by *Kiehl and Ramanathan* [1982], the 12- to 18-μm region for CO_2 absorption is overlapped by H_2O bands. Enhanced emission due to increased tropospheric CO_2 is partly compensated for by enhanced absorption due to increased H_2O. An increased water vapor concentration therefore enhances the tropospheric heating due to CO_2 and simultaneously reduces the surface heating due to CO_2. This effect was discussed in some detail by *Ohring and Joseph* [1978] and *Kiehl and Ramanathan* [1982], who analyzed the infrared cooling rates due to the combined effects of H_2O and CO_2. Ohring and Joseph studied the total cooling (from all bands) and also the cooling in the 15-μm CO_2 overlap region. Both CO_2 and H_2O alone act to cool the troposphere [*Plass*, 1956]. Ohring and Joseph found that with the addition of CO_2 to H_2O, the longwave cooling is less than it is with H_2O alone. H_2O is concentrated near the surface, and so emits radiation at lower levels than CO_2. Any radiation that is transmitted to space by the water vapor from lower tropospheric levels has another chance then to be absorbed by the CO_2 above, so there is a decrease in the cooling rate; a portion of the radiation has been trapped in the troposphere. In the stratosphere the overlap effect is small, so that the cooling rates due to CO_2 and H_2O are additive. The combination of CO_2 and H_2O thus causes stronger stratospheric cooling than either acting alone.

Figures 9 and 10 present the zonally averaged CO_2 forcing at the surface and at the CO_2 tropopause. These figures show the differences in the net upward infrared flux between $2 \times CO_2$ and $1 \times CO_2$ for both runs; negative values indicate reduced upward fluxes. At the surface, CO_2 forcing reduces the net upward flux by about 2 W m^{-2} in high latitudes, where there is little water vapor, but by less than 1 W m^{-2} near the equator, where water vapor absorbs the down-welling IR emitted by the CO_2 above [*Kiehl and Ramanathan*, 1982]. The global means are -1.24 W m^{-2} for the cold run and -0.86 W m^{-2} for the warm run.

The mean flux difference at the CO_2 tropopause is -4.33 W m^{-2}; the maximum reaches about -5 W m^{-2} in the tropics. In the warm run the mean is -4.59 W m^{-2} and a maximum of about 5.3 W m^{-2} occurs at 15°S. The smallest CO_2 forcing occurs at the winter pole (~ -2 W m^{-2}). There is a relative minimum near the equator, where high clouds block the upward infrared flux anyway.

Figures 11 and 12 are latitude-height plots of the clear-sky CO_2 forcing for the cold run and for the difference between the two runs. The most notable difference between Figures 7

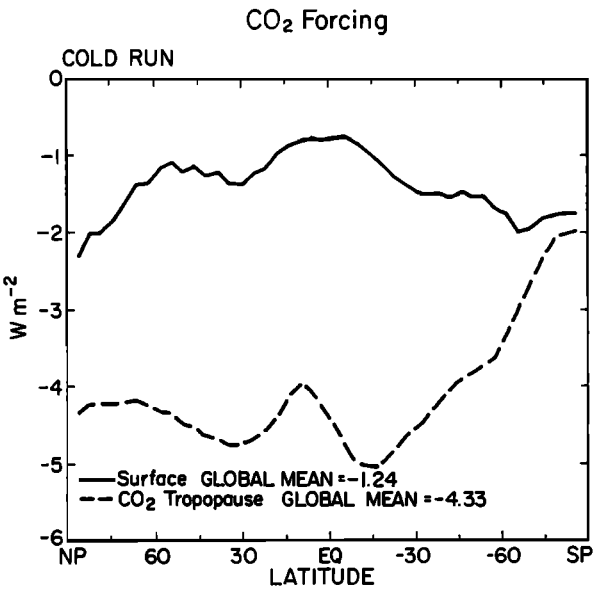

Fig. 9. Zonal means of the changes in flux at the Earth's surface and at the CO_2 tropopause, due to CO_2 forcing for the cold run.

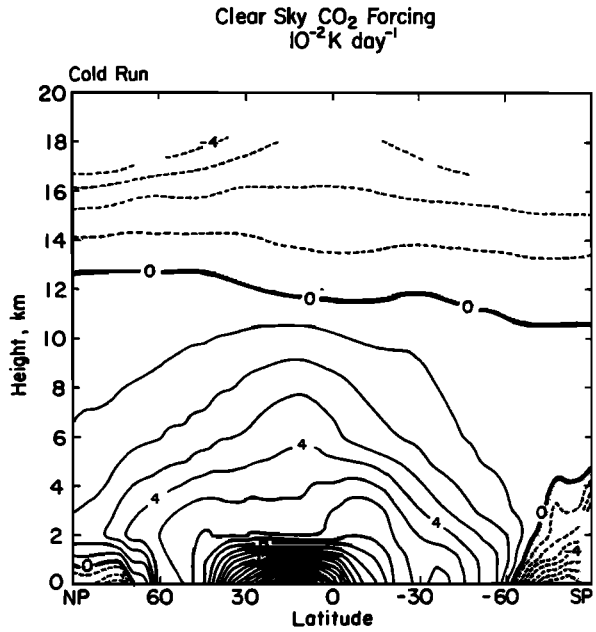

Fig. 11. Latitude-height distribution of the clear-sky CO_2 forcing for the cold run. Positive values indicate that the CO_2 forcing tends to warm.

and 11 is that the tropical "peak" in the CO_2 tropopause is missing in Figure 11 (the clear case). This demonstrates that the peak is caused by the effects of clouds. Figure 12 shows that the clear-sky CO_2 warming of the lower tropical troposphere is shifted upward in the warmer run. This is due to the increased water vapor of the warmer run; down-welling radiation emitted by CO_2 in the middle and upper troposphere is absorbed by water vapor at a higher level in the warmer run; less is then available for absorption near the surface.

Figures 13 and 14 directly show the effects of clouds on the CO_2 forcing. Figure 13 shows that in the tropical upper troposphere (above about 12 km), the high clouds shown in Figure 3 tend to convert the CO_2 forcing from a cooling (cf. Figure 11) to a weaker cooling or even a warming (cf. Figure 7), by absorbing the photons emitted by the CO_2. This effect is related to the tropical peak in the CO_2 tropopause, seen in Figure 7. In the lower troposphere, except near the south pole, the clouds reduce the CO_2 forcing in the cold run. This reduction is most noticeable in the tropics. The model produces many optically thick "anvil" clouds with their bases near the 8-km level [*Harshvardhan et al.*, 1989]; as seen in Figure 13, this is near the level at which the cloud modulation of the CO_2 forcing switches from an enhanced

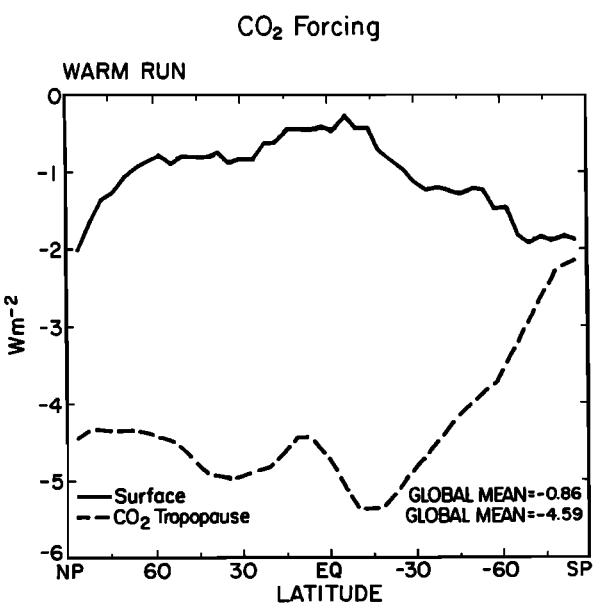

Fig. 10. Same as in Figure 9, but for the warm run.

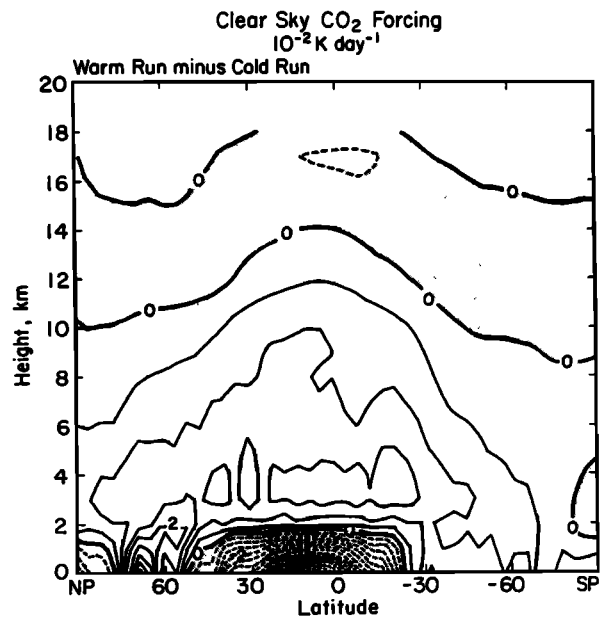

Fig. 12. Latitude-height differences (warm run minus cold run) in the clear-sky CO_2 forcing. Positive values indicate that the CO_2 forcing warms more (or cools less) in the warm run than in the cold run.

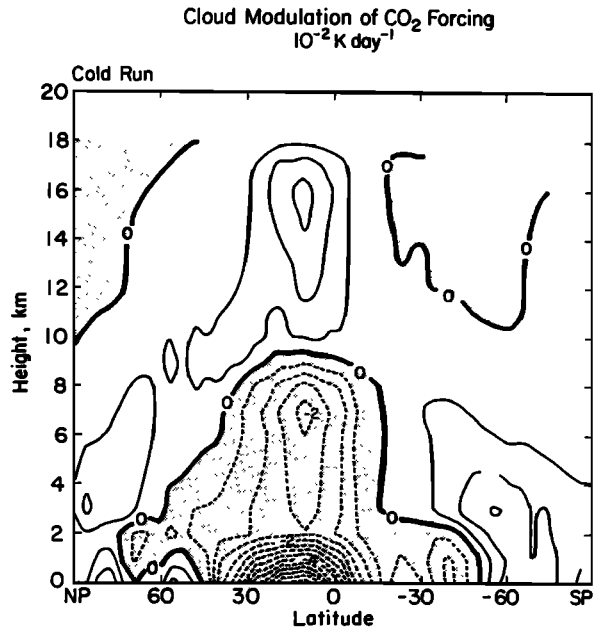

Fig. 13. Latitude-height plot of the cloud modulation of the CO_2 forcing for the cold run.

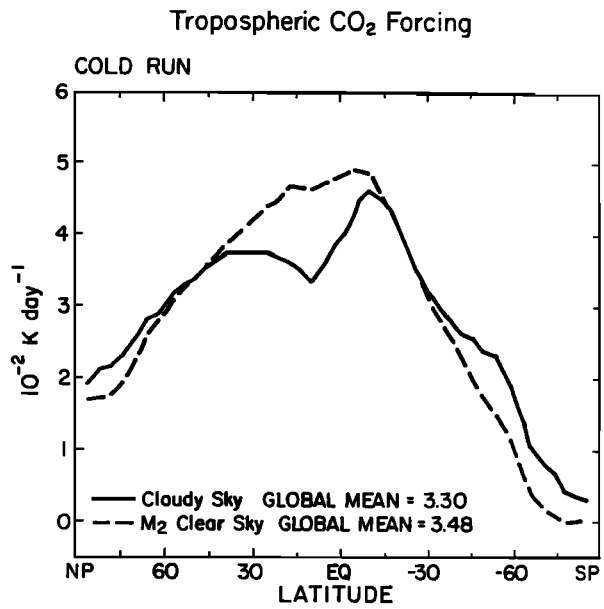

Fig. 15. Zonally averaged tropospheric heating due to the CO_2 forcing for both all-sky and clear sky for the cold run.

warming (above) to a weaker warming (below). Evidently, the upper tropospheric clouds are blocking downward radiation emitted by CO_2 above the 8-km level, thus preventing this radiation from being absorbed by the water vapor in the lower and middle troposphere. This effect is stronger in the middle tropical troposphere of the warm run, but weaker in the lower tropical troposphere of the warm run (Figure 14) because the increased water vapor of the tropical middle troposphere in the warm run has played somewhat the same role as the upper tropospheric clouds.

Figures 15 and 16 show the all-sky and clear-sky zonally averaged tropospheric CO_2 forcing, expressed as a heating rate, for the cold run and the warm run. Here we have taken into account the geographical variations of the surface pressure and the pressure at the CO_2 tropopause. The CO_2-induced tropospheric warming is stronger in the warm run. The most notable differences between the all-sky and clear-sky results occur in the tropics and in middle and high latitudes of the winter hemisphere. The CO_2-induced warming is reduced by the effects of clouds where high clouds dominate and is increased where low clouds dominate. Low and middle clouds, which are most prevalent at middle and high latitudes, tend to increase the CO_2 forcing across the troposphere by absorbing downward radiation emitted by CO_2 above cloud top. High clouds, on the other hand, tend

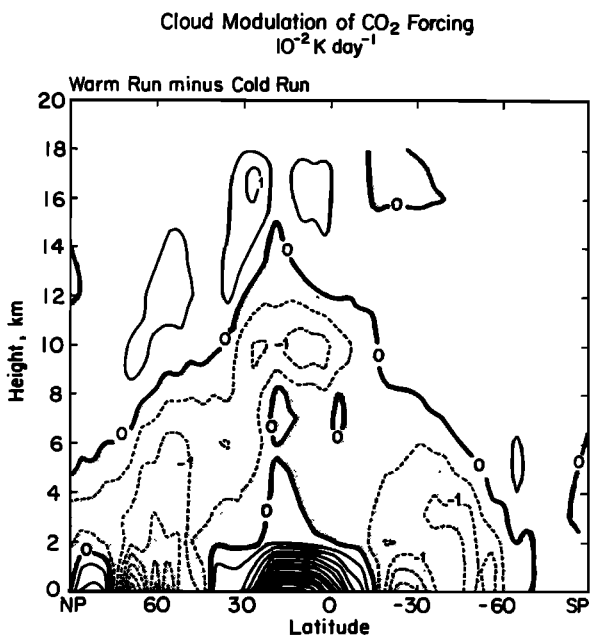

Fig. 14. Latitude-height differences (warm run minus cold run) in the cloud modulation of the CO_2 forcing.

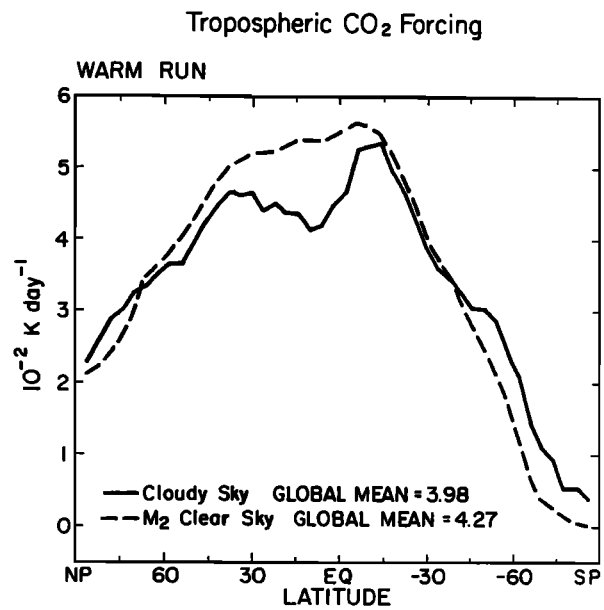

Fig. 16. Same as in Figure 15, but for the warm run.

TABLE 2. All-Sky and Clear-Sky CO_2 Forcing at the Earth's Surface and at the CO_2 Tropopause

Level	All Sky or Clear Sky	Run	Global Mean, W m^{-2}
Surface	all sky	cold	−1.24
		warm	−0.86
	clear sky	cold	−1.75
		warm	−1.20
CO_2 Tropopause	all sky	cold	−4.33
		warm	−4.59
	clear sky	cold	−4.99
		warm	−5.18

Numbers given are the change in the net upward longwave radiation due to doubling CO_2. Negative values indicate the CO_2 reduces the net upward longwave radiation.

to reduce the CO_2 forcing across the troposphere, because they absorb upwelling radiation that might otherwise be absorbed by CO_2.

For the globally averaged troposphere, the high cloud effects are dominant in the sense that the clouds reduce the CO_2-induced tropospheric warming. In particular, the high cloud effects are dominant in the tropics, where the model produces few low clouds. On the other hand, where both low/middle and high clouds occur, the overall effect of the clouds is to increase the CO_2-induced heating of the troposphere. This is the case from about 45°N poleward, and from 30°S poleward. There are few low and middle clouds in the tropics, so the high clouds dominate there, leading to a reduction in the CO_2 forcing. At 60°S, there is a maximum of middle and low clouds, which accounts for the strong tropospheric CO_2 forcing at that latitude.

SUMMARY AND CONCLUSIONS

We have examined the effects of SST and clouds on the CO_2 forcing. The overall effect of a warmer ocean is to decrease the CO_2 forcing at lower levels and to increase it at upper levels, leading to a net increase in the CO_2-induced heating of the troposphere and the Earth-atmosphere system, but a reduction in the CO_2 forcing of the Earth's surface. The temperature dependence of the CO_2 forcing comes about mainly through the temperature dependence of the hydrologic cycle, and in particular through the strong dependence of the precipitable water on SST. In fact, the differences between the warm and cold runs are most apparent in the hydrologic diagnostics. Water vapor effects dominate cloud effects.

Table 2 summarizes our results for the CO_2 forcing at the Earth's surface and at the CO_2 tropopause. There is more CO_2-induced surface heating in the absence of clouds. Low clouds, in particular, reduce the surface CO_2 forcing because they block the downward radiation from CO_2 above cloud top. The CO_2 forcing at the CO_2 tropopause also increases in the absence of cloud effects. Clouds block the upward infrared radiation anyway, so that CO_2 has nothing to do; take the clouds away, and the CO_2 plays a more important role.

The CO_2 forcing at the CO_2 tropopause is stronger in the warm run, because the warmer, less cloudy troposphere tends to emit more infrared radiation, allowing more infrared blocking by the CO_2. Note, however, that the net upward radiation at the CO_2 tropopause is stronger in the warm run.

The surface CO_2 forcing is actually weaker in the warm run. Since the warm atmosphere contains about 50% more water vapor, the increased downward tropospheric emission due to increased CO_2 is largely absorbed by H_2O before it can reach the surface. Note, however, that the downward emission by water vapor increases strongly in the warm run [*Ramanathan*, 1981], and of course this dominates. The net effect, then, is that the infrared cooling of the surface is weaker in the warm run, even though the surface CO_2 forcing is reduced.

Table 3 summarizes our results for the CO_2 forcing across the troposphere. In the warm run the CO_2 forcing is weaker at the surface and stronger at the CO_2 tropopause. As a result, the tropospheric CO_2 forcing is stronger in the warm run. For the troposphere and the atmosphere as a whole, the clouds reduce the magnitude of the CO_2 forcing.

Since, in the warm run, the CO_2 forcing is weaker at the surface but stronger at the CO_2 tropopause, the overall effect is that the tropospheric CO_2 forcing is stronger in the warm run. Note, however, that the tropospheric infrared emission by water vapor is also stronger in the warm run; since this effect easily dominates, the net infrared cooling of the troposphere is considerably enhanced in the warm run. The increased infrared cooling of the troposphere is balanced by the increased latent heating associated with the more vigorous hydrologic cycle [*Ramanathan*, 1981].

High tropical clouds reduce the CO_2-induced heating of the troposphere, and low-level polar clouds increase it. Globally, the high-cloud effects dominate. Overall, however, the effects of clouds are less important than those of water vapor in determining the differences in CO_2 forcing between the warm and cold runs.

Our results can be used to draw some tentative inferences concerning the feedback processes associated with a climate change. As summarized in Table 2, the prescribed SST increase leads to an increase in the CO_2 forcing at the CO_2 tropopause. Overall, this would appear to be a positive feedback, if the warming were actually due to a higher CO_2 concentration. The feedback is due to the effects of water vapor: the warmer atmosphere contains more water vapor, which increases the CO_2 forcing across the atmosphere. This result could have been qualitatively anticipated on the basis of *Ohring and Joseph*'s [1978] analysis of the radiative interactions between CO_2 and water vapor.

In our model the cloud amount at all levels slightly decreases as the SST increases. Since we have seen that, in an overall sense, clouds act to reduce the CO_2 forcing at the CO_2 tropopause, a reduction in cloudiness would tend to enhance the CO_2 forcing. This is, then, another positive feedback, and an aspect of the "cloud" feedback that, to our

TABLE 3. All-Sky and Clear-Sky CO_2 Forcing Across the Troposphere

All Sky or Clear Sky	Run	Global Mean, W m^{-2}
All sky	cold	3.30
	warm	3.98
Clear sky	cold	3.48
	warm	4.27

Positive values denote a warming.

knowledge, has not been previously recognized. Of course, changes in cloudiness can also affect the climate through many other mechanisms.

Our results are qualitatively consistent with those of the earlier study by *Ramanathan et al.* [1979]. This is remarkable, given the many differences between the two studies, notably in the cloud and water vapor distributions used.

Our results for the CO_2 forcing are model-dependent, of course. Every GCM-based study of CO_2-induced climate change produces a CO_2 forcing, however, and the warming scenarios generated depend very directly on this forcing. A thorough investigation of the CO_2 forcings produced by GCMs is thus a rather basic prerequisite for understanding the climate change predictions produced by the models. It would be interesting to compare our CO_2 forcing results with similar calculations derived from other GCMs, for which the simulated cloud and water vapor distributions may be quite different.

Acknowledgments. This paper is based on Christina Schmitt's Master's thesis. Harshvardhan of Purdue University and Robert Cess of the State University of New York at Albany made helpful comments on the manuscript. Donald Dazlich assisted with running the GCM, and with the plotting. Support has been provided by NASA's Climate Program under grant NAG 5-1058, and later by the Department of Energy under contract DE-FG02-89ER69027. Computing resources have been provided by the Numerical Aerodynamic Simulation Facility at NASA Ames Research Center.

REFERENCES

Arakawa, A., and J.-M. Chen, Closure assumptions in the cumulus parameterization problem, *Short and Medium Range Numerical Weather Prediction, J. Meteorol. Soc. Jpn., Spec. Vol.*, pp. 107–131, 1987.

Arakawa, A., and W. H. Schubert, The interactions of a cumulus cloud ensemble with the large-scale environment, I, *J. Atmos. Sci.*, *31*, 674–701, 1974.

Cess, R. D., and G. L. Potter, Exploratory studies of cloud radiative forcing with a general circulation model, *Tellus*, *39A*, 460–473, 1987.

Cess, R. D., et al., Intercomparison and interpretation of cloud-climate feedback as produced by fourteen atmospheric general circulation models, *Science*, *245*, 513–516, 1989.

Cess, R. D., et al., Intercomparison and interpretation of climate feedback processes in ten atmospheric general circulation models, *J. Geophys. Res.*, *95*, 16,601–16,615, 1990.

Chou, M.-D., Broadband water vapor transmission functions for atmospheric IR flux computations, *J. Atmos. Sci.*, *41*, 1775–1778, 1984.

Chou, M.-D., and L. Peng, A parameterization of the absorption in the 15-mm CO_2 spectral region with application to climate sensitivity studies, *J. Atmos. Sci.*, *40*, 2183–2192, 1983.

Harshvardhan, R. Davies, D. A. Randall, and T. G. Corsetti, A fast radiation parameterization for general circulation models, *J. Geophys. Res.*, *92*, 1009–1016, 1987.

Harshvardhan, D. A. Randall, T. G. Corsetti, and D. A. Dazlich, Earth radiation budget and cloudiness simulations with a general circulation model, *J. Atmos. Sci.*, *46*, 1922–1942, 1989.

Intergovernmental Panel on Climate Change (IPCC), *Climate Change: The IPCC Scientific Assessment*, edited by J. T. Houghton, G. J. Jenkins, and J. J. Ephraums, 365 pp., Cambridge University Press, New York, 1990.

Kiehl, J. T., and V. Ramanathan, Radiative heating due to increased CO_2: The role of H_2O continuum absorption in the 12-18μm region, *J. Atmos. Sci.*, *39*, 2923–2926, 1982.

Ohring, G., and J. H. Joseph, On the combined infrared cooling of two absorbing gases in the same spectral region, *J. Atmos. Sci.*, *35*, 317–322, 1978.

Plass, G. N., The influence of the 15-μ carbon-dioxide band on the atmospheric infrared cooling rate, *Q. J. R. Meteorol. Soc.*, *82*, 310–323, 1956.

Ramanathan, V., The role of ocean-atmosphere interactions in the CO_2 climate problem, *J. Atmos. Sci.*, *38*, 918–930, 1981.

Ramanathan, V., M. S. Lian, and R. D. Cess, Increased atmospheric CO_2: Zonal and seasonal estimates of the effect on the radiation energy balance and surface temperature, *J. Geophys. Res.*, *84*, 4949–4958, 1979.

Randall, D. A., Harshvardhan, D. A. Dazlich, and T. G. Corsetti, Interactions among radiation, convection, and large-scale dynamics in a general circulation model, *J. Atmos. Sci.*, *46*, 1943–1970, 1989.

Randall, D. A., Harshvardhan, and D. A. Dazlich, Diurnal variability of the hydrologic cycle in a general circulation model, *J. Atmos. Sci.*, *48*, 40–62, 1991.

Roberts, R. E., J. E. A. Selby, and L. M. Biberman, Infrared continuum absorption by atmospheric water vapor in the 8-12 μm window, *Appl. Opt.*, *15*, 2085–2090, 1976.

Schlesinger, M. E., and J. F. B. Mitchell, climate model simulations of the equilibrium climatic response to increased carbon dioxide, *Rev. Geophys.*, *25*, 760–798, 1987.

D. A. Randall and C. Schmitt, Department of Atmospheric Science, Colorado State University, Fort Collins, CO 80523.

(Received November 30, 1990;
revised March 4, 1991;
accepted March 4, 1991.)